Analyses of hydraulic performance of velocity caps

Christensen, Erik Damgaard; Degn Eskesen, Mark Chr.; Buhrkall, Jeppe; Jensen, Bjarne

Published in:
Book of Proceedings

Publication date:
2014

ANALYSES OF HYDRAULIC PERFORMANCE OF VELOCITY CAPS

ERIK DAMGAARD CHRISTENSEN (1), MARK CHR. DEGN ESKESEN (2), JEPPE BUHRKALL(2) & BJARNE JENSEN(1)

(1) Technical University of Denmark, Kgs. Lyngby, Denmark, edch@mek.dtu.dk

(2) Present address: Ramboll Oil and Gas, Denmark

Abstract

The hydraulic performance of a velocity cap has been investigated. Velocity caps are often used in connection with offshore intakes. CFD (computational fluid dynamics) examined the flow through the cap openings and further down into the intake pipes. This was combined with dimension analyses in order to analyse the effect of different layouts on the flow characteristics. In particular, flow configurations going all the way through the structure were revealed. A couple of suggestions to minimize the risk for flow through have been tested.

Keywords: Offshore intake; Velocity cap; CFD-analyses

1. Introduction

Velocity caps are often used in connection with for instance offshore intake of sea water for cooling water in power plants or as a source for desalinization plants. The intakes can also be used for river intakes. The velocity cap is placed on top of a vertical pipe that leads the water into another pipe or tunnel system. A pressure gradient generated by the water level difference between the sea and basin drives the flow through the tunnel system. The tunnel system is often in the order of a couple of kilometers long.

There are several reasons to use a velocity cap:

- Avoid air-entrainment
- Reduce fish entrapment in the system
- Avoid intake of sediment into the system.

The objective of this study is to use computational fluid dynamics to examine the hydraulic performance of the velocity cap and the hydraulic system. For some layouts of velocity caps, the flow may go all the way through the velocity cap. This creates a very uneven velocity field around the structure that should be avoided as this might increase fish entrapment.

Alternative solutions such as direct intake of surface seawater are hampered by impingement and entrainment of planktonic organisms that require additional filtration and pretreatment. A general introduction to water intake structures can for instance be found in (ASCE, 1981).

During the last decade Computational Fluid Dynamics has become a reliable tool to investigate hydraulic problems. For instance (Tokyay & Constantinescu, 2006) used an advanced CFD-model to examine the flow in a pump-sump. (He, Wood, Marsalek, & Rochfort, 2008) used CFD to improve a storm-water clarifier. (Khan, Wicklein, & Rashid, 2005) used a three-

dimensional CFD-model to study an outfall structure, used for discharging 55 m^3/s of cooling water to a reservoir. The outfall consisted of two inflow pipes, two deflectors and a baffle wall.

This paper investigates the flow around, into and through a velocity cap, which often is a part of an offshore intake structure. The analyses were based on computational fluid dynamics. The basis for the CFD model was the open source library OpenFOAM®, see http://www.openfoam.org/index.php.

2. The velocity cap

A velocity cap is sketched in fig. 2.1. The diameter of the cap is denoted D_c, and the opening of the cap h_c. The vertical pipe that connects the velocity cap to the transport tunnel/pipe has a diameter of d_v, while the diameter of the transport pipe is d_h. The total water depth from the free surface to the seabed is d. In figure 2.2 the numbering of the openings is given for later reference.

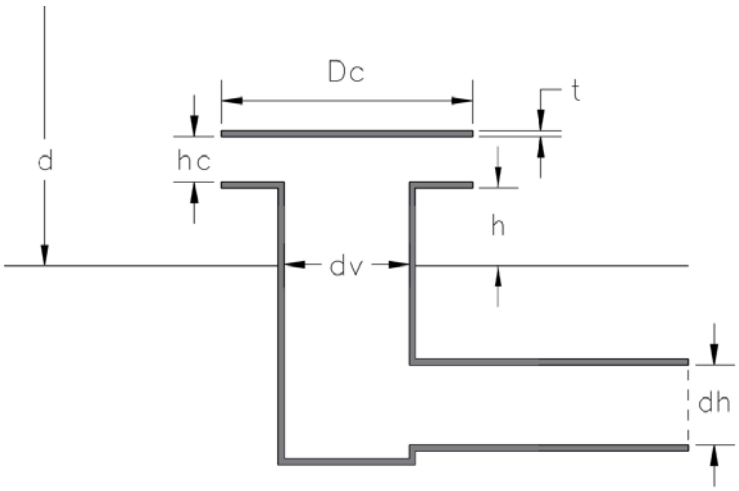

Figure 2.1 Vertical cross-section of the velocity cap

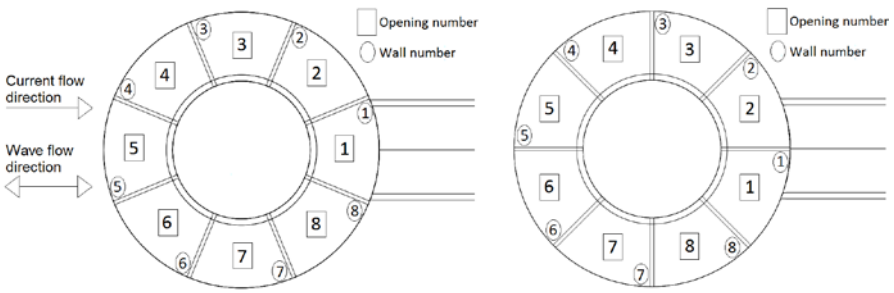

Figure 2.2 Horizontal cross-section of the velocity cap, Left: Opening and guiding wall notations. Right: Opening and guiding wall notations for skew flow direction

3. Methodology

3.1 Numerical method

The numerical method is based on a solution of the Reynolds Averaged Navier-Stokes (RANS) equations that for the continuity equation and for the momentum equations read:

$$\frac{\partial U_i}{\partial x_i} = 0 \tag{3.1}$$

$$\frac{\partial U_i}{\partial t} + U_j \frac{\partial U_i}{\partial x_j} = -\frac{1}{\rho}\frac{\partial p}{\partial x_i} + \frac{\partial}{\partial x_j}\left((\nu + \nu_t)\left(\frac{\partial U_i}{\partial x_j} + \frac{\partial U_j}{\partial x_i} \right) \right) \tag{3.2}$$

where U_i is the time averaged velocity in the ith direction, p is the pressure, ν is the kinematic viscosity, and the ν_t is the eddy viscosity.

The eddy viscosity arises from the closure problem during the averaging process. Here the Reynolds stresses were modelled based on the eddy viscosity concepts, meaning that the Reynolds stresses could be modelled as:

$$\tau_{ij} = \rho\overline{u_i u_j} = \rho\nu_t\left(\frac{\partial U_i}{\partial x_j} + \frac{\partial U_j}{\partial x_i} \right) \tag{3.3}$$

In eqs. (3.3) the eddy viscosity still have to be found. To this end a rather standard two-equation turbulence model was used, the SST k-ω-model(SST: Shear Stress Transport), see (Menter, 1993). This model has shown to give robust and reliable solutions to the flow field where adverse pressure gradient has to be considered. The flow into, and at times through, the velocity cap generates adverse pressure gradients. For the sake of completeness we also present the model equations for the turbulent kinetic energy, k, and the specific dissipation rate ω here:

$$\rho\frac{\partial k}{\partial t} + \frac{\partial \rho k U_i}{\partial x_j} = \frac{\partial}{\partial x_j}\left[\left(\mu + \mu_t \middle/ \sigma_k \right)\frac{\partial k}{\partial x_j} \right] + \tau_{ij}\frac{\partial U_i}{\partial x_j} - \rho\beta^* k\omega \tag{3.4}$$

$$\rho\frac{\partial \omega}{\partial t} + \frac{\partial \rho\omega U_i}{\partial x_j} = \frac{\partial}{\partial x_j}\left[\left(\mu + \mu_t \middle/ \sigma_\omega \right)\frac{\partial \omega}{\partial x_j} \right] + \frac{\gamma}{\nu_t}\tau_{ij}\frac{\partial U_i}{\partial x_j} - \beta\rho\omega^2 + 2(1-F_1)\frac{\rho\sigma_{\omega 2}}{\omega}\frac{\partial k}{\partial x_j}\frac{\partial \omega}{\partial x_j} \tag{3.5}$$

The constants σ_k, and σ_ω are found from the generic equation (3.6), where numbers 1, and 2 corresponds to the inner and outer regions. The constants, γ, β, β^*, σ_k, and σ_ω, for the inner and outer solutions can be found in table 1 and 2:

$$\phi = F_1\phi^1 + (1-F_1)\phi^2 \tag{3.6}$$

The blending function F_1 is a function of the distance to the wall:

$$F_1 = \tanh(\arg_1^4)$$

where

$$\arg_1 = \min\left[\max\left(2\frac{\sqrt{k}}{0.09\omega z};\frac{500\mu}{z^2\omega}\right);\frac{4\rho k}{(CD_{k\omega})z^2\sigma_{\omega 2}}\right] \tag{3.7}$$

with

$$(CD_{k\omega}) = \max\left(2\rho\frac{1}{\sigma_{\omega 2}\omega}\frac{\partial k}{\partial x_j}\frac{\partial \omega}{\partial x_j};10^{-20}\right)$$

Table 1. Model constants for inner 'wall' region

β_1	β^*	γ_1	σ_{k1}	$\sigma_{\omega 1}$
0.075	0.09	0.553	2.0	2.0

Table 2. Model constants for outer 'surface' region

β_2	β^*	γ_2	σ_{k2}	$\sigma_{\omega 2}$
0.0828	0.09	0.4404	1.0	1.17

Finally the following equation estimates the eddy viscosity used in the RANS-equations:

$$\nu_t = \frac{a_1 k}{\max(a_1\omega, \Omega F_2)} \tag{3.8}$$

Where is the rotation ($\Omega = (\frac{\partial U_i}{\partial x_j} + \frac{\partial Uj}{\partial x_i})$), and a_1 is a constant. F_2 is a blending function which is one for boundary layer flows and zero for free shear layers. Equation (3.8) ensures that the original eddy viscosity is only used outside the inner layer where adverse pressure gradients are rare.

$$F_2 = \tanh(\arg_2^2)$$

where (3.9)

$$\arg_2 = \max(2\frac{\sqrt{k}}{0.09\omega z};\frac{500\mu}{z^2\omega})$$

3.1.1 Solution method

The solution method is based on the open source library OpenFOAM (Open Field Operation and Manipulation): This is an open source, object-orientated C++ library for numerical simulations of fluid dynamics. See for instance (Jasak & Jemcov, 2007). The equations were solved on the computational mesh (see 3.1.2) using a velocity-pressure solver. The numerical integration in time was based on the PISO-algorithm using a Crank-Nicholsen method making the scheme close to second order in time. The Gauss linearUpwind (LUD) resolved the convective terms, while central differences was used for diffusive terms. This leads to a spatial resolution close to second order. The pressure equation that can be derived from the continuity equation was solved using preconditioned conjugated gradient solver (PCG), while the

momentum equations and the turbulence equations were solved using preconditioned bi-conjugate gradient solver (PBICG). As preconditioner the Diagonal Incomplete Cholesky (DIC) was used for the pressure, while diagonal incomplete LU (DILU) was used for the momentum and turbulence equations. More information can be found in (Eskesen & Buhrkall, 2013).

3.1.2 The computational grid

The computational domain is resolved by a number of computational cells forming the computational mesh. These cells can have different shapes such as triangles and rectangles in two-dimensions and tetrahedrals and hexahedrals in three-dimensions. The cells can either be structured or unstructured.

Setting up the computational mesh is often a key point of CFD and can be a complicated task. The procedure for the computational mesh used in this study was as follows. First a background mesh was generated using hexahedral cells. Hereafter the procedure for snappyHex was used, see for instance (Tapia, 2009). This method finds the intersection between the geometry of the structure and the hexahedral cells. Cells enclosed by the geometry were removed. The remaining cells that were neighbours to the structure were connected to the surface of the geometry by displacing cell-vertices onto the surface of the structure.

The end result was a computational mesh that was generated relatively fast and that included the structure in the computations. However the mesh cells at the surface of the structure might be too large to resolve the boundary layer at the surface.

3.1.3 Boundary conditions.

- Structure surface, top and bottom
  A slip condition was applied to the top structure (velocity cap) with zero pressure gradient and normal velocity. By adopting the slip conditions, the boundary layer close to the structure surface will not be resolved. However that would require a very fine mesh resolution as a too coarse resolution might make the solution unstable or simply produce unphysical results.
- Inlet (outer boundary of the computational domain) :
  <u>No ambient current:</u>
  All the sides were defined as inlet boundaries with zero normal gradient velocity and fixed value pressure, here zero. This allows the water to enter symmetrical and free into the domain.
  <u>With an ambient current</u>
  The upstream side was modelled as an inlet boundary, with zero pressure gradient and a fixed value velocity.
- Pipe outlet:
  An outlet boundary with a pressure gradient equal to zero and a fixed value normal velocity is applied to the end of the horizontal pipe. A constant velocity is applied to the entire plane and depends on the desired discharge. The fixed value velocity is chosen instead of the pressure since it provides better control of the discharge.

3.2 Dimension analyses

In order to perform a meaningful and systematic analysis, dimensional analysis was adopted. The dependent variable was the intake velocity U_{in}, while the important independent variables of the process, within the scope of the study, were identified as:

$$U_{in} = f\left[U_c;\ Q;\ h_c;\ D_c;\ d_v\right] \tag{3.10}$$

Obvious the external flow velocity U_c and the discharge Q will influence the intake velocity.

Intake velocities depend on the dimensions of the velocity cap, i.e. D_c and h_c. Since the dimension of the vertical pipe affects the appearance of the velocity cap, the diameter of the vertical pipe d_v, should be included as well.

Several other variables might be regarded as important but still not included in the dimensional analysis. The location of the intake, h, could affect the intake symmetry and turbulence level at the velocity cap. If the intake is situated near the seabed the majority of the intake water will come from above, due to the proximity of a boundary. Furthermore the current velocity decreases towards the seabed. It was assumed that the location, h, only will be important if it is small, i.e. if the velocity cap is close to the seabed. This will often be out of the range where most velocity caps are located. The water depth, d, is another important variable which is omitted. It is assumed that the depth is only important for situations with low water-level.

Apart from the external and geometric variables, three material variables could be relevant. The density and temperature are two material variables which could be of importance. The temperature and density dependencies were omitted in order to limit the scope of the analyses. The viscosity is another material variable that could affect the intake flow. For small Reynolds numbers, the velocity profile inside each opening will depend upon the viscosity. The viscosity is discarded since it is assumed that the flow will be governed by turbulence and strong wake creation rather than Reynolds effects. The separation takes place at sharp corners. Therefore the geometry of the structure will have the largest effect of the generation of separation cells. Finally by omitting any mass quantities the problem is solely a kinematic problem, see (Hughes, 1993).

3.2.1 Dimensionless products

From the dimensional analysis, the 6 variables are reduced to 4 dimensionless products:

$$\pi\frac{U_{in}h_cD_c}{Q} = f\left(\frac{U_ch_cD_c}{Q}, \frac{h_c}{D_c}, \frac{d_v}{D_c}\right) \tag{3.11}$$

The product $\pi U_{in}h_cD_c / Q$ will be referred to as the relative discharge and corresponds to the ratio between the local intake discharge and the required total discharge Q. The relative discharge can be regarded as a measure of the velocity distribution around the velocity cap. If it is equal to one the situation corresponds a flow that is evenly distributed around the velocity cap. However if the ratio is different from unity an asymmetric situation is created. The product $U_ch_cD_c / Q$ will be named the relative momentum and may be interpreted as a measure of the horizontal momentum relative to the vertical momentum inside the vertical pipe. It is convenient to use the relative momentum to assess the impact of the external variable, e.g. flow-through and velocity distribution. The aspect ratio of the openings h_c / D_c is

a measure of the flow conditions inside the velocity cap. A small ratio corresponds to a long slender channel with parallel flow; hence viscous effects may be important and visa verse. The ratio d_v/D_c is a measure of how far the water needs to travel before the flow changes direction.

4. Results

Some of the result will be presented and discussed in the following. Further details can be found in (Eskesen & Buhrkall, 2013). In the following the analyses focus on the effect of an ambient current on the flow distribution into the velocity cap.

4.1 Internal flow separation

At the guiding walls the separation cells and stagnation regions are formed as expected. The separation cells which develop in the side openings increases with the current speed and may eventually block the entire intake opening. As a result the flow is redirected around the velocity cap, cf. figure 4.1 (b) and (d). Figure 4.1 (d) illustrates how the flow separates around the velocity cap creating a wake region. The effect of the intake flow in the openings is seen by the way they prevents the inner layers from separating. The internal flow separation plays an important role in terms of the distribution of velocities. Figure 4.1 (d) illustrate how the flow separation creates a free stream jet, which concentrates and directs the flow out of opening (1). In addition a vortex redirects the flow around opening (2).

4.1.1 Redistribution of velocities

The flow resistance, found at the upstream openings induces a redistribution of the intake velocities. As a result, the largest velocities are found at the side openings. This is further enhanced by the separation cells formed behind the guiding walls. Since these reduce the active intake area, the local velocities are concentrated. At some point certain separation cells will block the entire opening; hence a further redistribution will take place. In these cases the flow will experience the velocity cap as an enclosed disk which causes contraction of streamlines. Consequently, the velocities increase at the sides of the velocity cap cf. figure 4.1 (d).

The relationship between the relative discharge $\pi U_{in} h_c D_c / Q$ and the relative momentum $U_c h_c D_c / Q$ can be examined from figure 4.2. As expected $\pi U_{in} h_c D_c / Q$ approaches unity for $U_c h_c D_c / Q \to 0$. This means that the intake discharge is evenly distributed between the eight openings. As $U_c h_c D_c / Q$ increases a redistribution of the relative discharge, $\pi U_{in} h_c D_c / Q$, takes place. Opening (4) and (5), which both are located with an angle less than 90° to the current, experience an increasing relative discharge, while a decrease is seen for the rest. The enhanced inflow found for opening (4) and (5) seems reasonable since the angle of these openings causes the guiding walls to capture the current flux. In line with this, opening (5) experiences the largest increase. Recall that the maximum velocities are not found at this opening, but due to the absence of separation cells the mean velocity or flux will be larger. Regarding opening (2) and (3) it is seen how these two follows an identical path, in which they experience a minor decrease. An examination of the separation cells and internal jets reveals the origin of this behaviour.

With increasing relative momentum the size of the separation cells grows, cf. figure 4.3. As a result the contraction area decreases, which causes the energy loss to increase. Eventually the

gradient of the discharge Q is too weak to drag in the flow into these openings. This explains the decrease down to zero, but not the negative values.

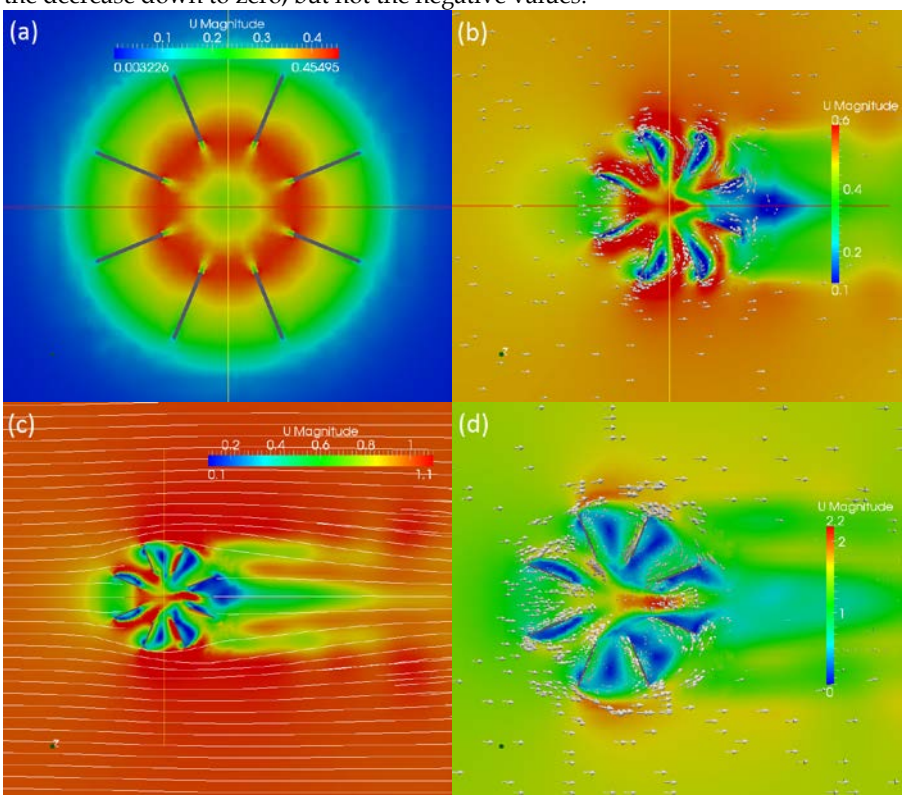

Figure 4.1. Horizontal slice through the center of the openings. h_c = 2 m, D_c = 11 m, Q = 15m^3/s , (a) velocity contours U_c = 0 m/s, (b) velocity contours U_c = 0.5m/s, (c) velocity contours U_c = 1m/s, (d) velocity contours U_c = 1.5 m/s.

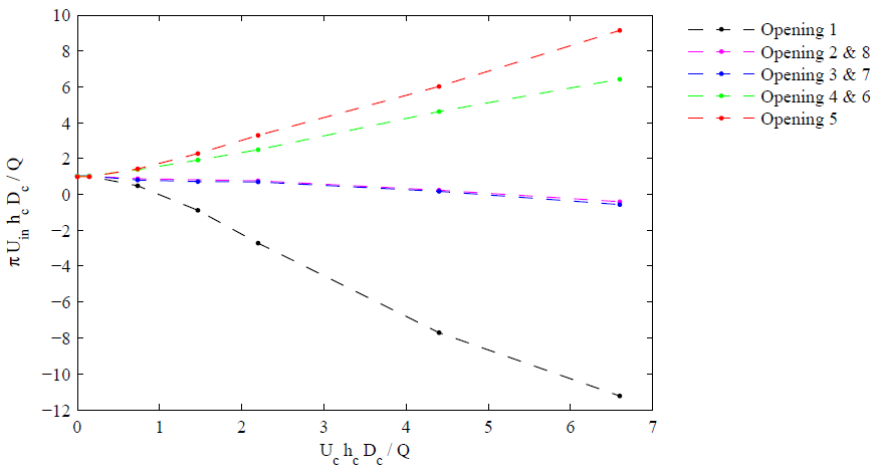

Figure 4.2. (4.8) Effect of the relative momentum with h_c/D_c = 0.18 and d_0/D_c= 0.5.

The negative values are a result of the internal jet and the separation cells. The internal free stream jets shields these openings from internal flows, cf. figure 4.3 (b). Meanwhile the flow separation forms a large recirculation cell that is driven by the external flow. In opening (3) a constant outgoing flux emerges, cf. figure 4.3 (b). While the recirculation cell induces a negative flux in opening (3), it generates a positive flux in opening (2).

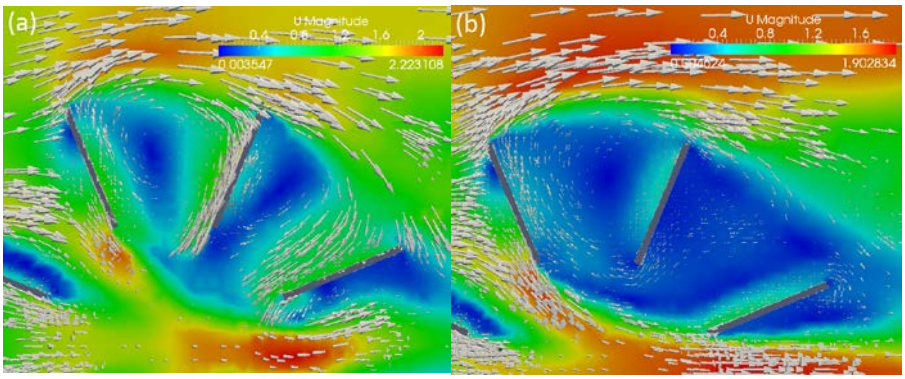

Figure 4.3 (4.9): Velocity contour for h_c = 2 m and D_c = 11 m opening (3) and (2). (a) Q = 15m³/s and U_c = 1.5 m/s, (b) Q = 5 m³/s and U_c = 1.5 m/s.

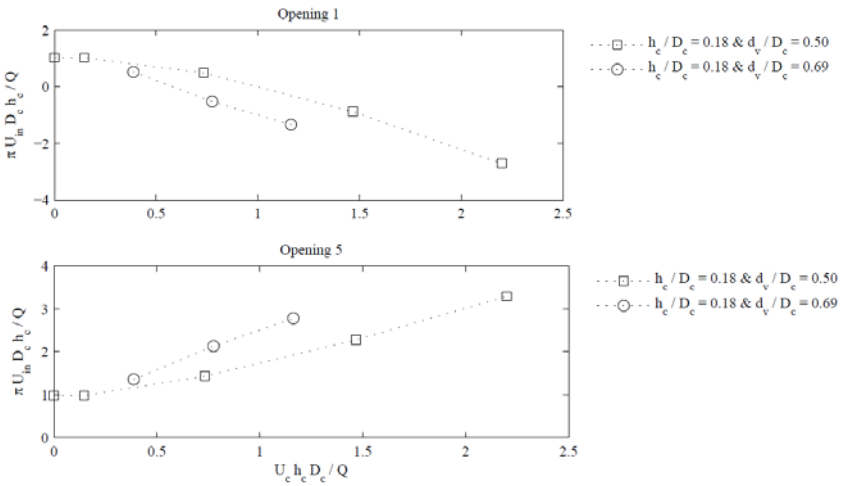

Figure 4.4 (4.11): Effect of aspect ratio d_v/D_c. (Vertical pipe diameter over diameter of velocity cap). Opening 1 is on the lee side and opening 5 confronting the incoming current.

An example of the effect of the aspect ratio between the vertical pipe diameter, d_v, and the diameter of the velocity cap, D_c, is shown in figure 4.4. When the ratio increases the flow through the velocity cap increases as well. This indicates that the flow through the intake can be minimized by lowering this ratio. However, this will typical lead to an increased total head loss that has to be accounted for in the design.

5. Conclusions

A CFD-model based on the open CFD-library OpenFOAM has been set up in order to analyse the hydraulic performance of velocity caps that often is an important part in offshore intake structures. The focus of the study has been on the effect of an ambient current on the distribution inflow. For larger ambient current speed a jet was formed by the guiding walls in the velocity cap that resulted in a negative inflow on the lee side of the velocity cap and larger inflow from the opposite side. The analyses showed that the effect can be reduced/enhanced if the ratio between the vertical pipe diameter and the diameter of the velocity cap, d_v/D_c, is reduced/enhanced.

References

ASCE (1981). *Design of Water Intake Structures for Fish Protection* (p. 163). New York.

Eskesen, M. C. D. E., & Buhrkall, J. (2013). *CFD analyses of Velocity Caps*. The Technical University of Denmark.

He, C., Wood, J., Marsalek, J., & Rochfort, Q. (2008). Using CFD Modeling to Improve the Inlet Hydraulics and Performance of a Storm-Water Clarifier. *Journal of Environmental Engineering*, *134*(9), 722–730. doi:10.1061/(ASCE)0733-9372(2008)134:9(722)

Hughes, S. A. (1993). *Physical models and laboratory techniques in coastal engineering* (Advanced S., p. 588). World Scientific Publishing Co. Pte. Ltd.

Jasak, H. (1996). Error Analysis and Estimation for the Finite Volume Method with Applications to Fluid Flows. *Direct*, *M*(June).

Jasak, H., & Jemcov, A. (2007). OpenFOAM : A C ++ Library for Complex Physics Simulations ˇ. In *International Workshop on Coupled Methods in Numerical Dynamics* (Vol. m, pp. 1–20). IUC, Dubrovnik, Croatia.

Khan, L. A., Wicklein, E. A., & Rashid, M. (2005). A 3D CFD model analysis of the hydraulics of an outfall structure at a power plant. *Journal of Informatics*, *7*(4), 283–290.

Menter, F. R. (1993). Zonal Two-Equation Kappa-Omega Turbulence Model for Aerodynamic Flows. In *AIAA 24th Fluid Dynamic Conference July 6–9* (pp. 93–2906). Orlando, Florida.

Tapia, X. P. (2009). *Modelling of wind flow over complex terrain using OpenFoam*. University of Gävle.

Tokyay, T. E., & Constantinescu, S. G. (2006). Validation of a Large-Eddy Simulation Model to Simulate Flow in Pump Intakes of Realistic Geometry. *Journal of Hydraulic Engineering*, *132*(12), 1303–1315. doi:10.1061/(ASCE)0733-9429(2006)132:12(1303)